Applied Catalysis B: Environmental 304 (2022) 120995

Contents lists available at ScienceDirect

Applied Catalysis B: Environmental

journal homepage: www.elsevier.com/locate/apcatb

Fluorine-doped iron oxyhydroxide cocatalyst: promotion on the WO_3 photoanode conducted photoelectrochemical water splitting

Yan Li [a,b], Qiong Mei [c], Zejun Liu [a], Xingsheng Hu [b], Zhaohui Zhou [a], Jingwei Huang [b], Bo Bai [a], Hui Liu [d], Fei Ding [a], Qizhao Wang [a,b,*]

[a] School of water and Environment, Key Laboratory of Subsurface Hydrology and Ecological Effects in Arid Region of Ministry of Education, Chang'an University, Xi'an 710054, China

[b] Gansu International Scientific and Technological Cooperation Base of Water–Retention Chemical Functional Materials, College of Chemistry and Chemical Engineering, Northwest Normal University, Lanzhou 730070, China

[c] School of land Engineering, Chang'an University, Xi'an 710054, China

[d] School of Metallurgy and Environment, Chinese National Engineering Research Center for Control & Treatment of Heavy Metal Pollution, Central South University, Changsha 410083, China

ARTICLE INFO

Keywords:
WO_3
$BiVO_4$
Photoelectrochemical water splitting
Fluorine doped FeOOH

ABSTRACT

WO_3 as a photoanode has the disadvantage of poor charge separation and low solar utilization. It is necessary to surmount these weaknesses to improve its performance. In this work, we doped FeOOH with F to prepare F:FeOOH/$BiVO_4$/WO_3 photoanode by the facile method. According to the photoelectrochemical evaluation, in the phosphate buffer electrolyte, the maximum photocurrent of the composite photoanode (3.1 mA/cm^2) is 7 times and 9 times that of WO_3 and $BiVO_4$, respectively. The improvement is ascribable to F:FeOOH can extract holes and improve charge transfer. Compared with $BiVO_4$/WO_3 and original components, F:FeOOH/$BiVO_4$/WO_3 photoanode enhances charge separation and also shows good stability and electrons lifetime. Additionally, F-doped FeOOH has better OER catalytic performance than FeOOH according to theoretical calculation, which is consistent with experimental results. This work might extend application of cocatalyst in decomposition PEC water splitting.

1. Introduction

In order to balance our long-term dependence on fossil fuels, it is urgent to research and develop efficient and environmentally friendly solar fuel conversion materials [1–3]. Photoelectrochemical (PEC) water splitting is considered as an effective method for the change from solar energy into hydrogen energy, which receives widespread attention [4,5]. Since the PEC water splitting hydrogen production with TiO_2 was put forward by Honda and Fujishima, many semiconductors were developed for PEC water splitting, particularly some metal oxide semiconductors (α-Fe_2O_3 [6,7], ZnO [8], $BiVO_4$ [9,10], WO_3 [11] etc.) were diffusely studied because of low toxicity, ample resources and low cost [12–15]. Among them, WO_3, in possession of suitable band gap (2.5–2.8 eV), medium diffusion length (~150 nm), satisfactory valence band (3.0 V vs. RHE) and appropriate electronic mobility (12 cm^2 V^{-1} s^{-1}) is a research hotspot in the field of PEC water splitting [16,17]. However, single WO_3 photoanode is limited by poor charge separation, rapid recombination of photoelectron-hole pairs, and low solar utilization [11,18,19]. These shortcomings can be improved by morphology control [20], heterojunction construction [21,22], surface modification [23,24], nanostructure engineering [25], doping [26], incorporation with oxygen evolution cocatalysts (OECs) [27] etc. Using two or more semiconductors to construct heterojunctions is reckoned as an effective approach to facilitate carrier separation and transport. In general, WO_3 could be combined with ZnO [28], Fe_2O_3 [29], $ZnWO_4$ [24], Bi_2S_3 [30], CdS [31], $BiVO_4$ [27] and other semiconductors to form heterojunction structures. $BiVO_4$ holds a narrow band gap (2.4 eV), namely, it is able to effectively absorb visible light, and considered to be a perfect candidate for bonding with WO_3 [32]. $BiVO_4$ has the more negative valence band (VB) and conduction band (CB) edges than WO_3. When WO_3 is coupled with $BiVO_4$, photo-generated electrons are readily transferred from the CB (+ 0.02 V vs. RHE) of $BiVO_4$ to that of WO_3 (+ 0.41 V vs. RHE), while

* Corresponding author at: School of water and Environment, Key Laboratory of Subsurface Hydrology and Ecological Effects in Arid Region of Ministry of Education, Chang'an University, Xi'an 710054, China.

E-mail address: wangqizhao@163.com (Q. Wang).

https://doi.org/10.1016/j.apcatb.2021.120995
Received 2 November 2021; Received in revised form 28 November 2021; Accepted 4 December 2021
Available online 7 December 2021
0926-3373/© 2021 Elsevier B.V. All rights reserved.

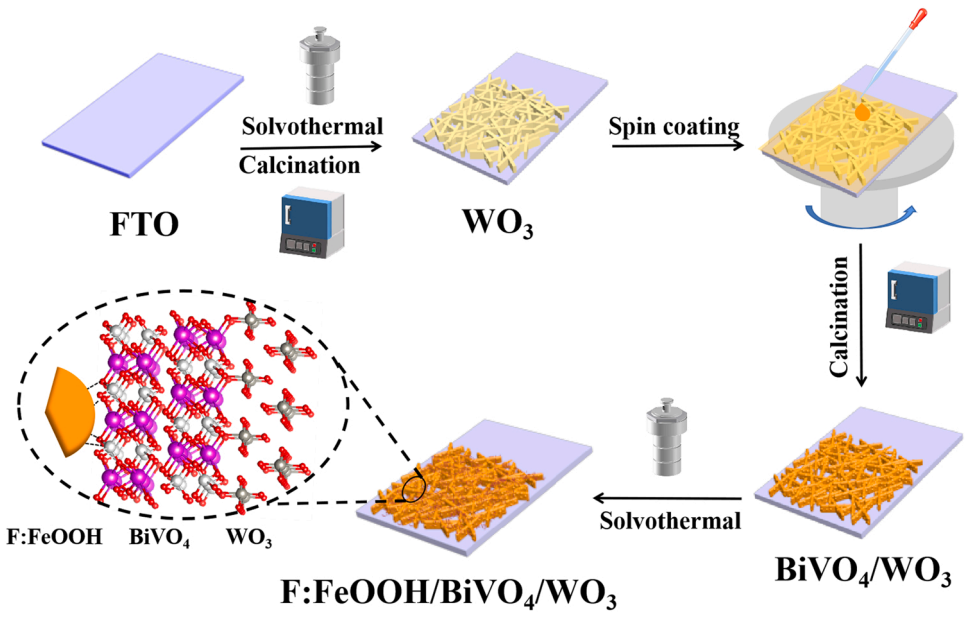

Fig. 1. The preparation process of F:FeOOH/$BiVO_4$/WO_3.

holes in $BiVO_4$ VB would migrate to the VB of WO_3 [33,34]. The reduction of carrier recombination in the coupling system ensures a greatly ameliorated PEC performance, that is, a significant enhancement for the separation of charges [35–37]. In addition to light absorption, charge separation and charge injection have a certain effect on the performance as well. The photoelectricity performance of $BiVO_4/WO_3$ is able to be ulteriorly lifted by supporting OECs, and the charge transfer kinetics can be improved [38,39]. Previous studies showed that rational deposition of OECs, e.g., CoO_x [21], FeOOH [40,41] and Sb_2S_3 [42] on the photoanode surface can promote charge injection capacity. OECs can not only speed up the surface reaction kinetics and decrease carrier recombination, but also inhibit the photoanode from directly contacting the electrolyte, thereby reducing photocorrosion and improving stability [43]. FeOOH is proved to be a highly active OER cocatalyst in the first transition metal [44,45]. However, the application of FeOOH is restricted by its poor electrical conductivity and high overpotential [46]. One of the efficacious ways to address the issue is doping cation or anion ions in/onto its bulk and surface position. For example, Chemelewski et al. reduced the overpotential of FeOOH by doping Ni, showing excellent PEC performance [47]; Through facile hydrothermal method, Cai's group prepared the Ni:FeOOH cocatalyst to surficially load on $WO_3/BiVO_4$ photoanode [48]. The photocurrent density was significantly increased and the initial potential was apparently negative shifted, indicating that this method bears a good application prospect. Fluorine (F), the most electronegative element, induces a positive charge density at the FeOOH iron site, thereby increasing OER activity [49].

In previous reports, traditional deposition annealing method was usually used to prepare $BiVO_4/WO_3$ heterojunctions. The process requires repeatedly heating and cooling [50]. In this work, two solutions of bismuth nitrate and peroxovanadate were alternately deposited on WO_3 film to fabricate $BiVO_4/WO_3$ photoanode by one-step calcination method. The PEC performance of $BiVO_4/WO_3$ is greatly lifted rather than that of either pure WO_3 or $BiVO_4$ photoanode. In addition, FeOOH was prepared as a cocatalyst with the modification of doping F element. The photoelectrochemical assessments imply that the photocurrent density of F:FeOOH/$BiVO_4/WO_3$ photoelectrode is 3.1 mA/cm^2, ca. 3 and 7 times that of $BiVO_4/WO_3$ electrode and pristine WO_3 photoanode, respectively. The initial potential of F:FeOOH/$BiVO_4/WO_3$ electrode is significantly negative shifted by 200 mV compared to pure WO_3. By contrast to $BiVO_4/WO_3$, the IPCE value of F:FeOOH/$BiVO_4/WO_3$ photoanode is also significantly lifted. Furthermore, the injection efficiency and the separation efficiency of F:FeOOH/$BiVO_4/WO_3$ respectively reache 74.4% and 66.8% at 1.23 V_{RHE}. The promoter, F:FeOOH, is capable of extracting holes and fosters the delivery of holes to the electrode surface/electrolyte interface for further participation in water oxidation reaction. These excellent properties may be attributed to the strong electronegativity of fluorine, which induces a positive charge density at the iron sites in the cocatalyst. According to theoretical calculation results, F-doped FeOOH should have better OER catalytic performance than FeOOH, which is consistent with experimental results.

2. Experimental

2.1. Materials

All chemical reagents are analytical grade and deionized water is used in all experiments. FTO conductive glass was purchased from Zhuhai Kaiwei Optoelectronics Technology Co., Ltd. $Na_2WO_4.2\ H_2O$, $FeCl_3.6\ H_2O$, $Bi(NO_3)_3.5\ H_2O$, NH_4VO_3, Na_2SO_3, HCl, H_2O_2 were purchased from Sinopharmacy Chemical Reagent Co., Ltd. $(NH_4)_2C_2O_4$ was purchased from Tianjin Kaixin Chemical Co., Ltd. Ammonium molybdate was purchased from Tianjin Kaida Chemical Plant. NH_4F and $NaNO_3$ were purchased from Shuangshuang Chemical Co., Ltd., Yantai City and acetic acid from Lian Long Bohua Pharmaceutical and Chemical Co., Ltd.

2.1.1. Preparation of $BiVO_4/WO_3$ photoanodes

The detailed preparation process of WO_3 can be seen in the support information. The $BiVO_4/WO_3$ electrode was prepared by spinning calcination. Firstly, 2.43 g $Bi(NO_3)_3.5\ H_2O$ was transferred to 2 M acetic acid solution and 0.585 g NH_4VO_3 was dissolved in 0.1 M H_2O_2 solution to prepare the peroxide solution. Typically, 100 μL of $Bi(NO_3)_3.5\ H_2O$ solution was dripped to WO_3 film at 2500 r.p.m. for 15 s. Similarly 100 μL of peroxovanadate solution was added to the film. This process is considered a cycle, and 15 cycles are typically used. The $BiVO_4/WO_3$ photoanode was obtained by annealing at 450 °C for 2 h. For comparison, $BiVO_4$ photoanode was prepared using the same process for 20 cycles.

2.1.2. Preparation of F:FeOOH/$BiVO_4/WO_3$

Typically, 0.16 g $FeCl_3.6\ H_2O$, 0.102 g $NaNO_3$ and 0.022 g NH_4F was added to 40 mL deionized water, and then transferred to the

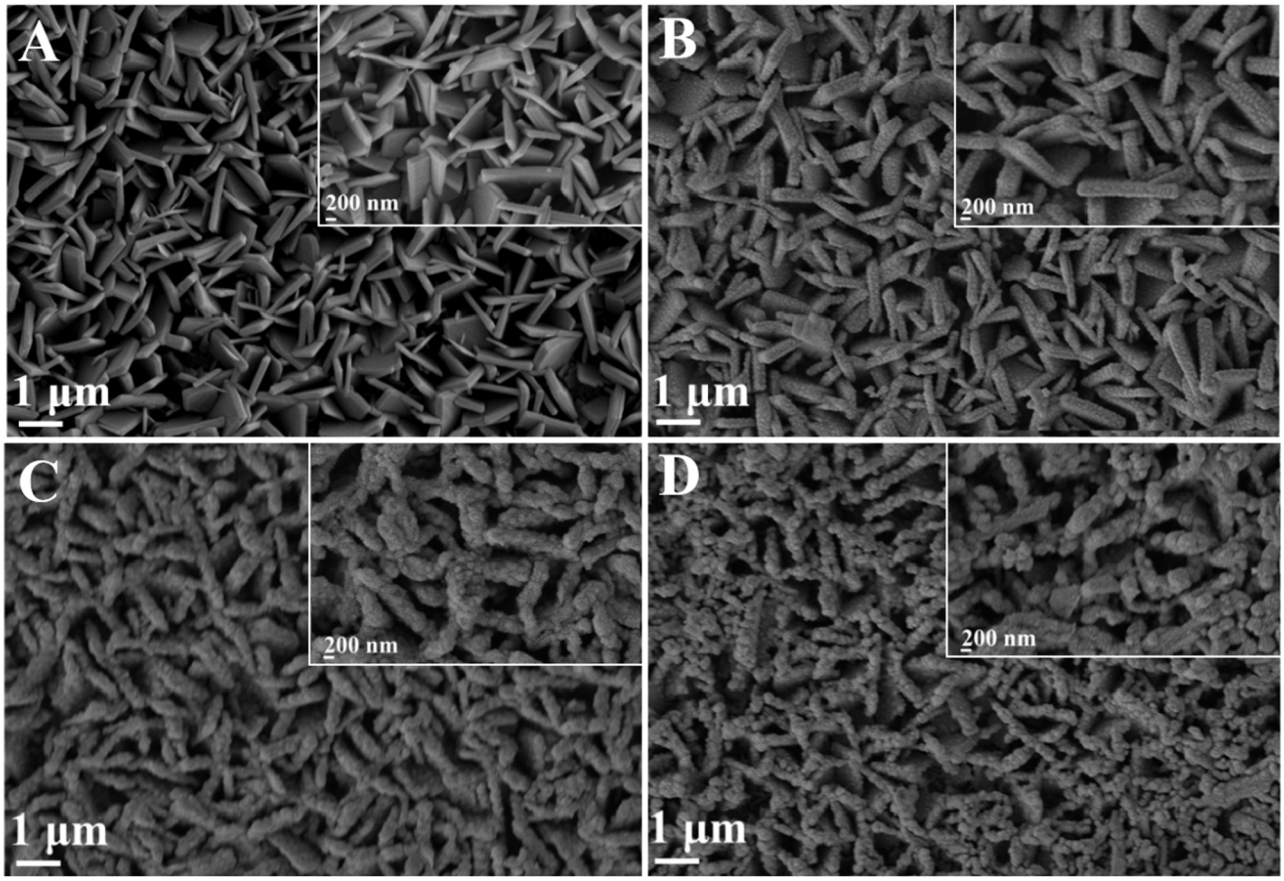

Fig. 2. SEM images of WO_3 (A), $BiVO_4/WO_3$ (B), $FeOOH/BiVO_4/WO_3$ (C), $F:FeOOH/BiVO_4/WO_3$ (D).

polypropylene bottle and hydrothermal reaction at 100 °C for 10 min. After being naturally reached to room temperature, rinse the photoanode with deionized water and dry in the air. The $FeOOH/BiVO_4/WO_3$ photoanode was prepared by a similar method except the solution without NH_4F.

2.2. Characterizations

The crystal structure of the prepared electrode was tested on X-ray diffraction (Rigaku D/Max-2200, CuKα radiation). The X-ray photoelectron spectroscopy (Thermo ESCALAB 250XI) was used to analyze chemical state and elemental components of the photoelectrodes. The morphology of the photoanodes was tested by scanning electron microscope (Zeiss Ultra Plus). Transmission electron microscope (Tecnai F30) was applied to study the microstructures. The UV-Vis spectra of the electrodes were tested by UV-Vis photospectrometer (Shimadzu UV-3600 Plus).

2.3. Photoelectrochemical measurements

All the performance tests of Photoelectrochemical water splitting have been carried out on the electrochemical workstation CHI660D with Ag/AgCl (3.5 M KCl) electrode as a reference electrode, Pt as a counter electrode and the photoanode as a working electrode. The electrolyte was 0.1 M KPi buffer solution with pH= 7 and 1 M sodium sulfite was used as holes scavener. A 300 W Xe lamp (PerfectLight, China) was adopted, with filter (AM 1.5G) as the illuminant, and calibrated optical power density was 100 mW/cm^2.

3. Results and discussion

3.1. Material structure and characterization

WO_3 nanoplates were grown on FTO substrate by hydrothermal method, and $BiVO_4/WO_3$ film (denoted as $BiVO_4/WO_3$) was formed by spin coating method (Fig. 1). F-doped FeOOH (F:FeOOH) was fabricated by hydrothermal method to prepare as a cocatalyst, which was further supported on the heterojunction (abbreviated as $F:FeOOH/BiVO_4/WO_3$). The morphology and nanostructure of the WO_3 electrode was investigated by the scanning electron microscopy (SEM) at low magnification and high magnification (Fig. 2A). The WO_3 nanoplate arrays were densely arranged on the FTO substrate. As depicted by Fig. 2B, WO_3 nanoplates are uniformly coated by $BiVO_4$ nanoparticles with a core-shell structure, $BiVO_4/WO_3$ formed after coating and annealing treatment. Besides, the comparatively smaller particles of FeOOH can be apparently observed on the $BiVO_4/WO_3$ surface, as shown in the Fig. 2C. The morphology of F-doped FeOOH cocatalyst was virtually unchanged due to small amount (Fig. 2D). In addition, the element mapping of the prepared $F:FeOOH/BiVO_4/WO_3$ (Fig. S1) confirms the presence of W, V, Bi, O, F and Fe elements in the structure, with no impure elements, indicating that the composite photoanode was successfully prepared.

To deeply investigate structural features of the samples, transmission electron microscope (TEM) was exerted. As shown in Fig. S2A, the surface of pure WO_3 is relatively smooth. The lattice fringe spacing is 0.38 nm that agrees with the (002) plane of WO_3 (Fig. S2B). According to the TEM of $F:FeOOH/BiVO_4/WO_3$ electrode (Fig. S2C), WO_3 is surrounded by $BiVO_4$ with the formation of a core-shell structure, and the outermost layer is coated with tiny F:FeOOH nanoparticles, which would facilitate the rapid migration of the holes. The lattice fringes corresponding to (1 2 1) plane of $BiVO_4$ can be observed from the high-

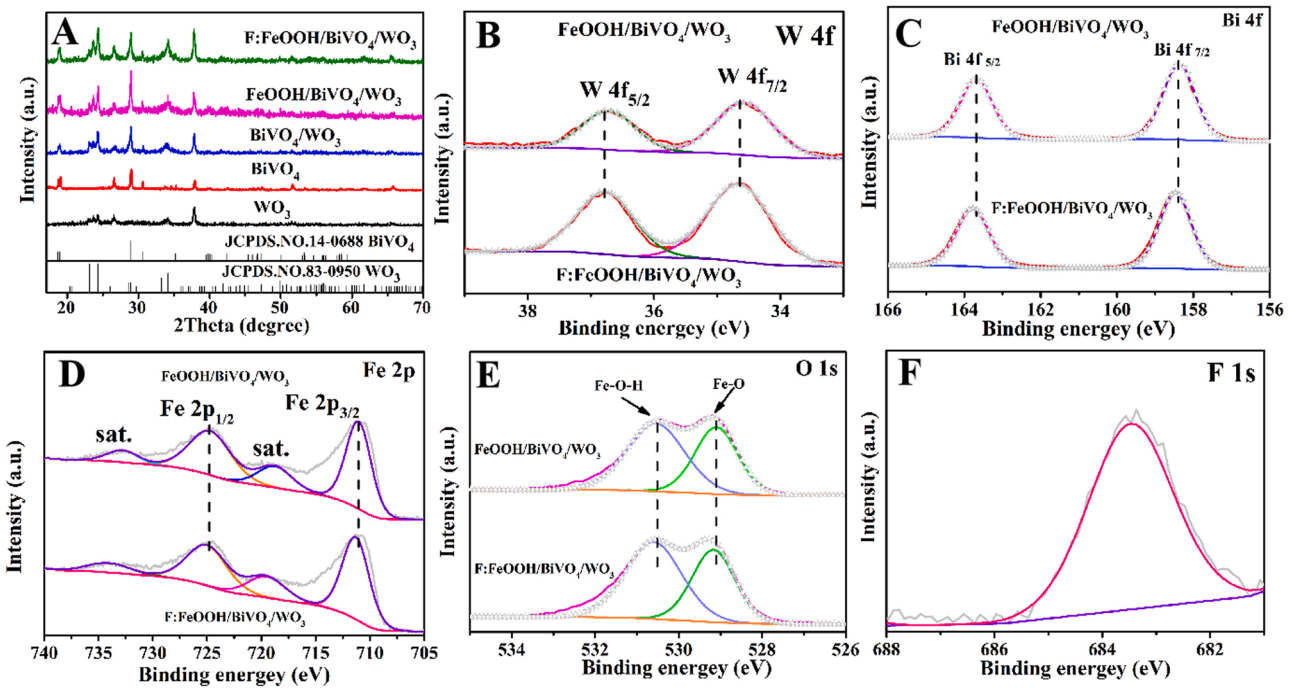

Fig. 3. XRD patterns of photoanodes (A); XPS spectra of W 4f (B), Bi 4f (C), Fe 2p (D), O 1s (E) of $FeOOH/BiVO_4/WO_3$ and $F:FeOOH/BiVO_4/WO_3$, F 1s (F) of $F:FeOOH/BiVO_4/WO_3$.

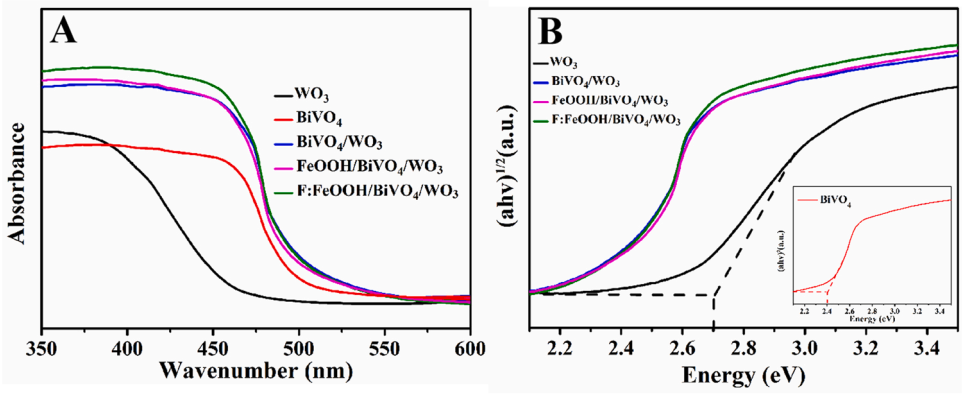

Fig. 4. UV-Vis absorption spectroscopy (A) and the band gap of the photoanodes (B).

resolution transmission image of the $F:FeOOH/BiVO_4/WO_3$ electrode (Fig. S2D).

X-ray diffraction (XRD) was applied to survey the crystal structures. As profiled in Fig. 3A, all the diffraction peaks are well correlated with WO_3 (JCPDS No.83–0950). The peaks located at 23.1°, 23.6°, 24.4° can be assigned to the (0 0 2), (0 2 0) and (2 0 0) planes of WO_3, respectively. In addition, the peaks at 18.9°, 28.6°and 30.5°corresponding to the (0 1 1), (- 1 3 0) and (0 4 0) crystal planes of $BiVO_4$, severally. After coating the FeOOH and F:FeOOH, the diffraction peaks show no obvious change, which may be attributed to less content of the cocatalysts.

X-ray photoelectron spectroscopy (XPS) tests, can study the chemical valence of substance, were executed on $FeOOH/BiVO_4/WO_3$ and $F:FeOOH/BiVO_4/WO_3$ electrodes (Fig. S3A). The emission spectrums of W 4f are shown in Fig. 3B. The peaks of $F:FeOOH/BiVO_4/WO_3$ discovered at 35.3 eV and 37.5 eV are in agreement with W $4f_{7/2}$ and W $4f_{5/2}$ of W^{6+}, respectively. The Bi 4f peaks of $F:FeOOH/BiVO_4/WO_3$ are situated at 163.8 eV and 158.5 eV, in keeping with Bi $4f_{5/2}$ and Bi $4f_{7/2}$ of Bi^{3+}, respectively (Fig. 3C). The W 4f and Bi 4f of $F:FeOOH/BiVO_4/WO_3$ move about 0.1 eV to the higher binding energy. In addition, in the V 2p spectrum of $F:FeOOH/BiVO_4/WO_3$, the V $2p_{1/2}$ and V $2p_{3/2}$ are located at 523.7 eV and 516.2 eV, respectively, certifying the existence of V^{5+} in $BiVO_4$ (Fig. S3B). The Fe 2p peaks of $F:FeOOH/BiVO_4/WO_3$ are 725.2 eV and 711.3 eV corresponding to Fe $2p_{1/2}$ and Fe $2p_{3/2}$ (Fig. 3D), at the same time, two satellite peaks are noticed, indicating that Fe exists as Fe^{3+}. The O 1s peak of $F:FeOOH/BiVO_4/WO_3$ observed at 529.3 eV is in connection with the metal-oxygen bonds of WO_3 and $BiVO_4$, and the peak at 530.8 eV is put down to the OH^- in F:FeOOH (Fig. 3E). The binding energies of Fe 2p and O 1s of $F:FeOOH/BiVO_4/WO_3$ also transfers to the higher binding energies. The changes of binding energy positions can be attributable to the strong electronegativity of F [44]. F 1s is detected at 683.5 eV (Fig. 3F). The results indicate that F: FeOOH was triumphantly prepared.

The UV-Vis absorption spectroscopy can investigate the optical properties of the photoanode. The absorption boundary position of WO_3 electrode is about 450 nm (Fig. 4A). After forming a heterojunction with $BiVO_4$, the light absorption intensity is intensified, and the absorption edge position presents a red shift. The light absorption intensity is further enhanced after FeOOH and F-doped, indicating that the

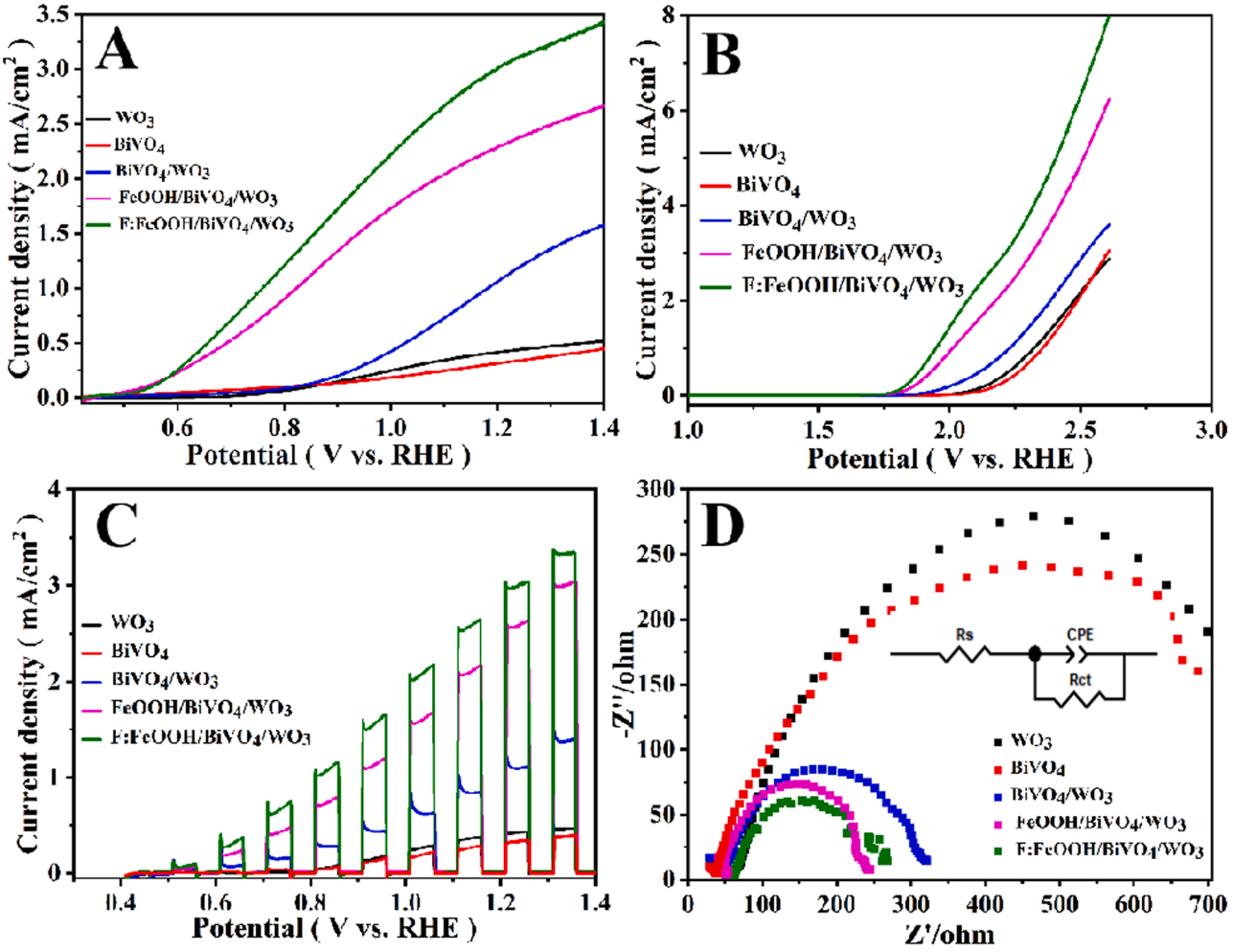

Fig. 5. Photocurrent density versus applied potential curves of electrodes (A), LSV curves of electrodes under the condition of dark reaction (B), transient photocurrent density of electrodes under chopped light (C), electrochemical impedance spectroscopy (EIS) of electrodes (D).

cocatalyst can effectively increase the response capacity of visible light and promote visible light absorption. In Fig. 4B, the band gaps are computed according to the Tauc equation, resulting in the band gaps of WO_3 and $BiVO_4$ as 2.69 eV and 2.4 eV, respectively, which are in a good consistence with previous reports. According to previous reports, the apparent electrochemical active area and catalytic active sites of OER are proportional, and the electrochemical double-layer capacitance (Cdl) could evaluate the apparent electrochemical active area. Relative electrochemical surface areas of electrodes are determined by the capacitance region of the cyclic voltammetry (Fig. S4A, C). The active areas of the electrode materials can be represented by linear relationship between the capacitance current and the scanning rate (Fig. S4B, D). After supporting the F:FeOOH cocatalyst, the active area slightly increases, which would promotes the water oxidation reaction.

3.2. PEC performance evaluation

The photoelectrochemical performance of the prepared photoanodes was tested in a representative three-electrode electrolytic cell. The prepared samples were subjected to the linear sweep voltammetry (LSV) in 0.1 M phosphate buffer electrolyte. According to the LSV tests of $BiVO_4/WO_3$ with different calcination times and cycles at 450 ℃, the best calcination time and cyclesof $BiVO_4$ are 2 h and 20 cycles at 450 ℃ (Fig. S5A, B). The reaction temperature and time of the F:FeOOH cocatalyst are optimized as shown in Fig. S5 C, D. We conclude that the optimal reaction temperature is 100 ℃ and the reaction time is 10 min. Subsequent cocatalysts were prepared under this condition. As displayed in Fig. 5A, the photocurrent density of F:FeOOH/$BiVO_4/WO_3$ photoelectrode at a potential of 1.23 V vs. RHE is 3.1 mA/cm^2, which is far better than $BiVO_4/WO_3$ (1.2 mA/cm^2), pure $BiVO_4$ (0.33 mA/cm^2) and pure WO_3 (0.43 mA/cm^2). According to Table S1, it is also known that the performance of WO_3-based heterojunction of this work is relatively excellent. Compared with the pure WO_3 electrode, the onset potential of the photoelectrodes with FeOOH cocatalyst and with F-doped FeOOH cocatalyst has a negative shift of about 200 mV. Under the condition of dark reaction, the initial potential of F:FeOOH/$BiVO_4/WO_3$ is lower than that of FeOOH/$BiVO_4/WO_3$, $BiVO_4/WO_3$ and WO_3, indicating that the water oxidation kinetics of photoanode is improved, as is shown in Fig. 5B. Fig. 5C shows the linear scanning curves of different electrodes under chopping wave illumination. The photocurrent density of the F:FeOOH/$BiVO_4/WO_3$ electrode is higher than that of other electrodes, which is consistent with the results in Fig. 5A. Furthermore, all electrodes have good optical switching characteristics and fast response. In particular, the response ability of the F:FeOOH/$BiVO_4/WO_3$ electrode in the low potential region is better than other electrodes. In addition, the curves of the transient photocurrent density over time were measured at 1.23 V vs. RHE. Under each irradiation, all samples of the photocurrent rise sharply. Once light is cut, it will quench to zero (Fig. S6A). The results show that the photocurrent of F:FeOOH/$BiVO_4/WO_3$ is significantly enhanced compared to the others, indicating that the F:FeOOH can enhance the separation of the photo-generated carriers.

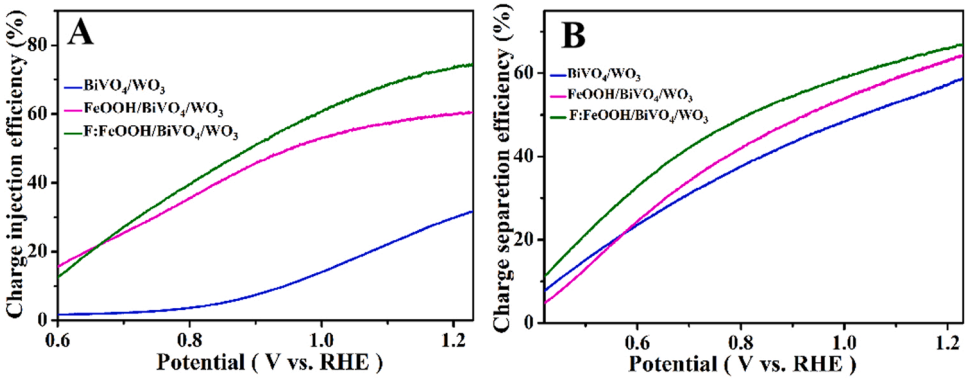

Fig. 6. Charge injection efficiency of electrodes (A) and charge separation efficiency of electrodes (B).

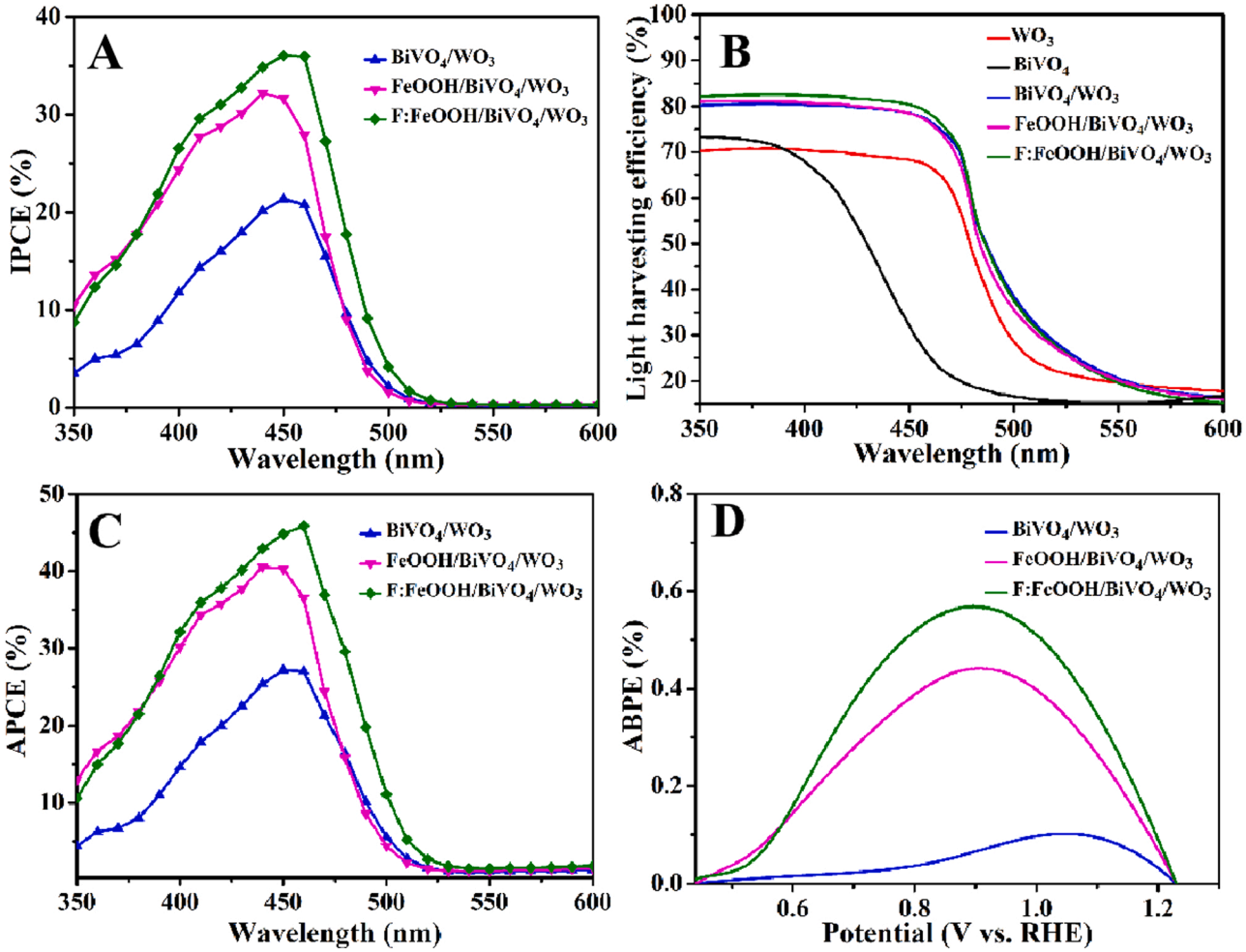

Fig. 7. IPCE (A), LHE (B), APCE (C) and ABPE (D) of photoanodes.

To investigate the rate of the charge migration, electrochemical impedance spectroscopy (EIS) was executed. According to Nyquist diagram (Fig. 5D, S6B), the electrode impedance arc radius decreases significantly after loading the cocatalysts with and without light, indicating that charge transfer is promoted. In addition, the illustration shows the equivalent circuit, where Rs is the solution resistance, CPE is the phasing element, and Rct is the charge transfer resistance at the electrode/electrolyte interface. It can be seen from Table S2 that the charge transfer resistance (Rct) of F:FeOOH/$BiVO_4$/WO_3 is the lowest, indicating that the modification of F is beneficial to charge transfer and promotes electrons and holes separation.

In order to visually display the surface charge injection efficiency, we also measured the photocurrent of the electrode when Na_2SO_3 was added as a hole scavenger in 0.1 M phosphate buffer (Fig. S6C). The surface charge injection efficiency is obtained by calculation. As shown in Fig. 6A, the surface injection efficiency of FeOOH/$BiVO_4$/WO_3 electrode reaches 60.4% at 1.23 V vs. RHE, and the injection efficiency reaches 74.4% at 1.23 V vs. RHE after F-doped. It shows that the promoter can extract holes and promote the transfer of holes to the photoanode surface/solution interface to take part in the water oxidation

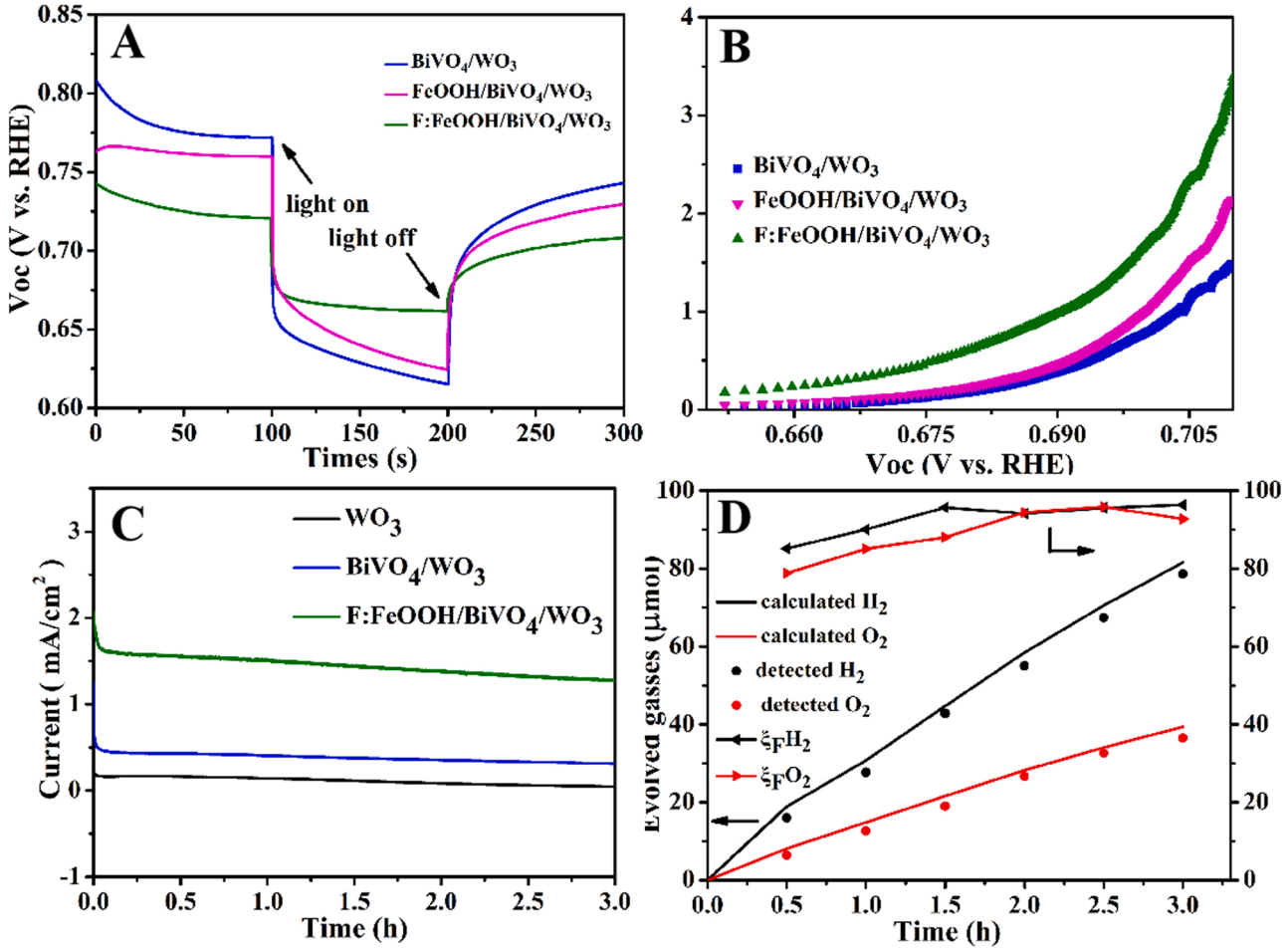

Fig. 8. Open-circuit photovoltage (Voc) versus time curves (A) and electron lifetimes of photoanodes (B); The stability test curves of F:FeOOH/$BiVO_4$/WO_3, $BiVO_4$/WO_3, WO_3 photoanodes (C) and the actual and theoretical H_2 and O_2 evolution and the Faradaic efficiency of F:FeOOH/ $BiVO_4$/WO_3 (D).

reaction. As can be seen from Fig. 6B that the photo-generated charge separation efficiency of F:FeOOH/$BiVO_4$/WO_3 electrode (66.8% at 1.23 V vs. RHE) is much higher than that of other electrodes, indicating that the loading of cocatalyst can ameliorate the charge separation efficiency and reduce recombination of electron and hole, thus immensely improving the PEC performance.

The incident photon-to-current efficiency (IPCE) is a very important index to study the optical conversion efficiency. By measuring the photocurrent with monochromatic light at 1.23 V vs. RHE, the IPCE of different photoanodes are analyzed. As shown in Fig. 7A, all photoanodes have a light response within a wavelength of 500 nm, which is consistent with the UV–vis absorption spectrum. At 450 nm, the IPCE of the $BiVO_4$/WO_3 photoanode is 21.3%, while the IPCE of the prepared F:FeOOH/$BiVO_4$/WO_3 photoanode is 36.0%, which is about 1.7 times. Obviously, the cocatalyst can inhibit the surface reorganization of the photo-generated charges, thereby improving the kinetics of water oxidation. Fig. 7B is a light harvesting efficiency (LHE) diagram, in the range of 350–600 nm, the light absorption efficiency of F:FeOOH/$BiVO_4$/WO_3 and FeOOH/$BiVO_4$/WO_3 electrodes are higher than that of WO_3 electrodes. The absorbed photon-to-current efficiency (APCE) of the electrodes can be calculated from the incident photonic current efficiency and light capture efficiency of the electrode, as shown in Fig. 7C. The maximum APCE value of F:FeOOH/$BiVO_4$/WO_3 photoanode is 45.86% at 460 nm, which is higher than that of other photoanodes. In order to evaluate the solar energy conversion efficiency in PEC water splitting process, a comprehensive comparative analysis of the applied bias photon-to-current efficiency (ABPE) of the prepared samples under the condition of applied bias voltage was carried out, as shown in Fig. 7D. The ABPE of pure WO_3 is 0.1% at 1 V vs. RHE, and the ABPE of $BiVO_4$/WO_3 heterojunction is also relatively increased. The ABPE value of the composite photoanode increases greatly after the cocatalyst loaded. The optimal ABPE value of F:FeOOH/$BiVO_4$/WO_3 photoanode is about 0.57% at 0.89 V vs. RHE, which is greater than FeOOH/$BiVO_4$/WO_3, $BiVO_4$/WO_3, $BiVO_4$ and WO_3, indicating that the supported catalyst can improve the photoactivity of OER.

To further explore the electron recombination dynamics of photoanodes, the decay of open circuit voltage (Voc) with time under AM 1.5 G irradiation was implemented (Fig. 8A). The photoelectric voltage decay rate is related to the electron lifetime derived from the equation (In the supporting information). The F:FeOOH/$BiVO_4$/WO_3 photoanode has a greater average carrier lifetime compared with others, indicating that the decay rate of the electrode is relatively slow, and the photo-generated electrons and holes are separated more efficiently (Fig. 8B).

The stability of the photoanode is an important reference for evaluating whether it has application value. Therefore, corresponding stability tests were carried out for the F:FeOOH/$BiVO_4$/WO_3, $BiVO_4$/WO_3, WO_3 photoanodes. The photocurrent of the composite electrode has no significant attenuation after continuous testing for 3 h under the light irradiation condition of AM 1.5 G, indicating that it has good stability (Fig. 8C). The amount of hydrogen and oxygen produced of the F:FeOOH/$BiVO_4$/WO_3 photoanode was measured by a gas chromatograph, as shown in Fig. 8D. During the reaction for 3 h, it can be clearly observed that the actual production amounts of hydrogen and oxygen are 78.6 μmol and 36.5 μmol, and the molar ratio of hydrogen and

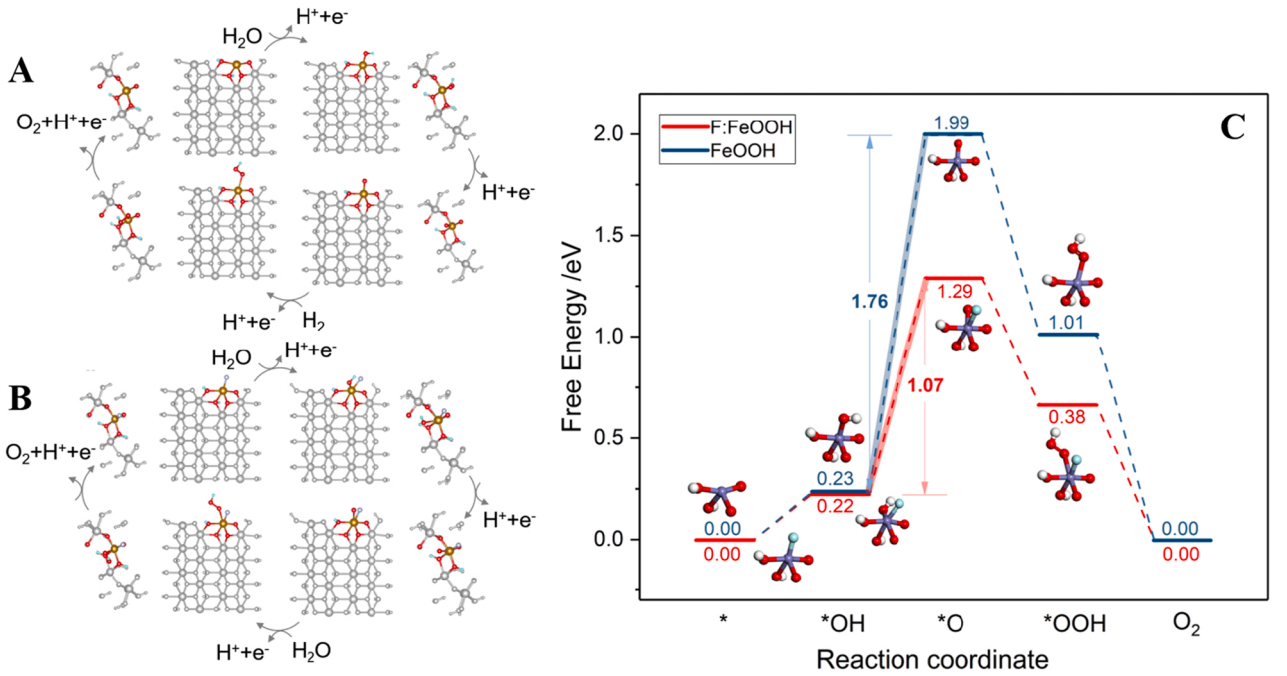

Fig. 9. The optimized configurations and reaction paths of OH* , O* , and OOH* adsorbed on FeOOH (A) and F:FeOOH (B) for OER. The corresponding free energy diagrams of each step of OER at 1.23 V potential (C).

oxygen is about 2:1. After calculation, the Faraday efficiency of hydrogen production and oxygen production are both about 96%. Based on the above test results, it can be seen that the F:FeOOH/$BiVO_4$/WO_3 composite photoanode has an excellent catalytic water splitting effect.

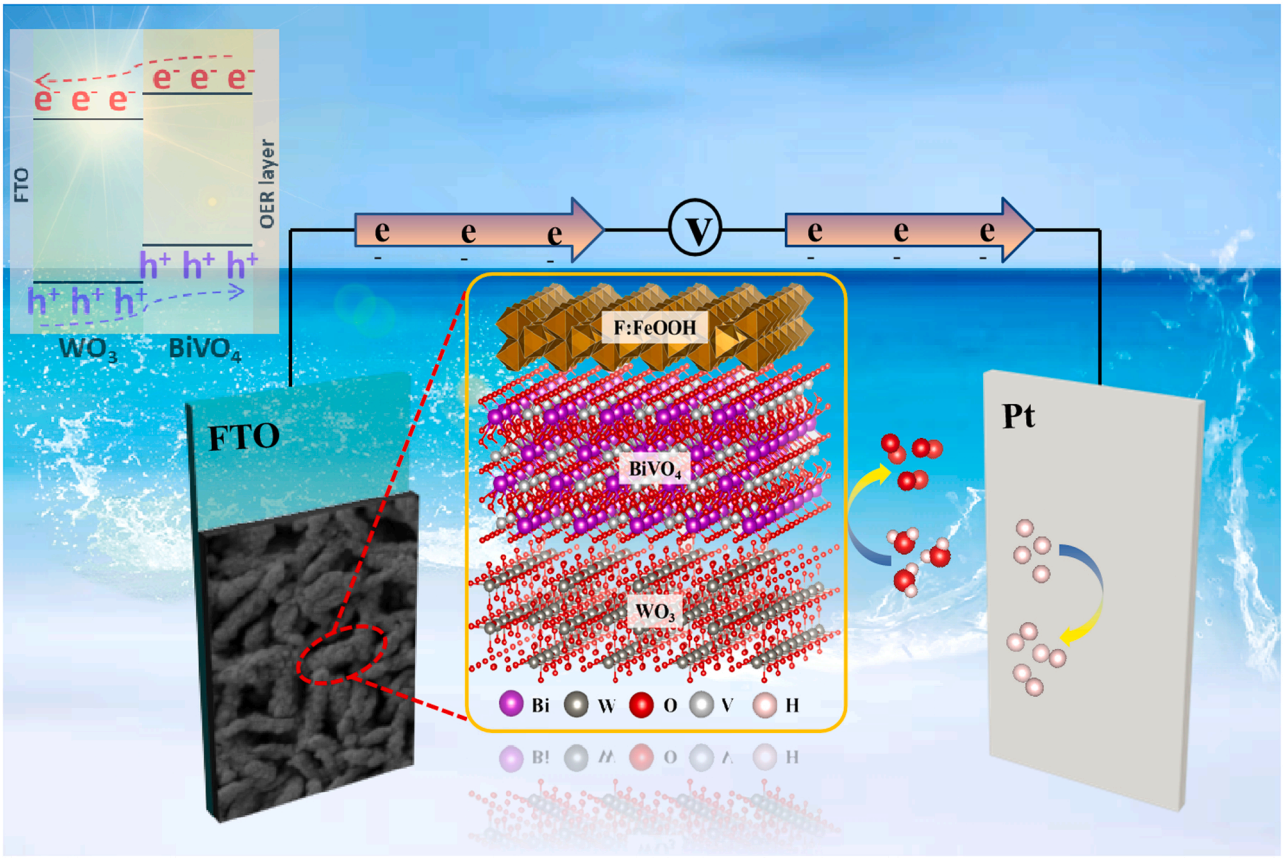

Fig. 10. The water oxidation mechanism diagram of photoanode.

3.3. Theoretical simulation

In this work, FeOOH (010) and F-doped FeOOH (010) surfaces were selected to study the OER process that occur on the surface in order to understand the effect of F atoms on the photocatalytic OER activity and energy of FeOOH surfaces. The OER mechanism in acidic media as follows [51]:

$$* + H_2O\ (l) = OH* + H^+ + e^- \quad (1)$$

$$OH* = O* + H^+ + e^- \quad (2)$$

$$O* + H_2O\ (l) = OOH* + H^+ + e^- \quad (3)$$

$$OOH* = * + O_2\ (g) + H^+ + e^- \quad (4)$$

* represents the adsorption sites of the surface, and OH* , O* , and OOH* represent the corresponding adsorption intermediates. The catalyst will enter the next cycle when O_2 was released from the surface of the catalyst. The overall OER reaction can be expressed as:

$$* + 2\ H_2O\ (l) = O_2\ (g) + 4\ H^+ + 4e^- \quad (5)$$

The optimized configurations and reaction paths of the major adsorption intermediates on the surface of FeOOH and F:FeOOH in the four-step OER process are shown in Fig. 9A and B. The free energy change diagram of the OER on the two surfaces at U= 1.23 V by DFT calculation (Fig. 9C). It is obvious from the optimized configurations that the local symmetry of Fe increases after OER, and the energy of slab also increases. As can be seen from the Fig. 9A and B, the second step of OER is the speed-determining step. For FeOOH and F:FeOOH, the free energy change from OH* to O* is the largest, and energy of 1.76 eV and 1.07 eV are required to complete the transformation of OH* and O* , respectively. Thus, the overpotential of FeOOH and F:FeOOH are 1.76 V and 1.07 V, respectively. Compared with FeOOH, the synergistic effect between Fe and S plays a significant role in stabilizing the adsorption intermediates, making the more negative free energy of OER on F:FeOOH. The calculation result shows that F-doped FeOOH should have better OER catalytic performance than FeOOH, which is consistent with the experimental results. It is worth noting that the F modification brings about steric effects and local electron rearrangement effects. The introduction of more F atoms does not necessarily reduce the free energy of the reaction.

3.4. Possible mechanism research

In order to study the reasons for the enhancement of PEC activity, the Mott-schottky (MS) measurements at different frequencies were performed on the electrodes in the absence of light. The flat band potential (V_{fb}) of electrodes can be obtained from the X-axis intercept from the MS diagram. Generally speaking, the semiconductor V_{fb} is related to its Fermi level (E_F), while the CB edge of n-type semiconductor is close to E_F. According to the MS diagram (Fig.S7), all slopes of electrodes are positive, indicating that they are n-type semiconductors, and the V_{fb} score of F:FeOOH/$BiVO_4$/WO_3 is more negative than that of others. Therefore, it means that electrons can flow from the cocatalyst layer to WO_3 step-by-step.

According to the above results, we imagined the probable charge transfer mechanism of F:FeOOH/$BiVO_4$/WO_3 photoanode, as shown in Fig. 10. First of all, $BiVO_4$ not only provides excellent light capture capability, but also provides an effective way for photoinduced electron-hole pairs separation and transfer. Secondly, when pure WO_3 nanoplate arrays are covered with dense $BiVO_4$ nanoparticles, a heterojunction will be formed. The photo-generated electrons are readily transferred from the CB of $BiVO_4$ to the CB of WO_3, and the photo-generated holes in the VB of $BiVO_4$ migrate to the VB of WO_3, thereby lifting the charge separation efficiency. In addition, the water oxidation performance is boosted ulteriorly by loading F-doped FeOOH cocatalyst. The reasons are as follows: the conduction position of F:FeOOH is more negative than that of $BiVO_4$ and can be well matched, facilitating the migration of photo-generated electrons from the CB of F:FeOOH to the CB of $BiVO_4$, while the electrons transferred from $BiVO_4$ to WO_3 are easily transported through the FTO substrate, forming an external circuit and improving the charge separation efficiency. The positive charge density of Fe sites is enhanced due to the strong electronegativity of F, which promotes the release of oxygen. In summary, the significant improvement of the photoelectricity water oxidation performance of the F:FeOOH/$BiVO_4$/WO_3 system is mainly caused by the formation of WO_3 and $BiVO_4$ and the introduction of F:FeOOH layer.

4. Conclusions

In summary, a highly efficient and stable F:FeOOH/$BiVO_4$/WO_3 photoanode was prepared on the FTO glass substrate for PEC water oxidation by means of hydrothermal reaction, spin coating and subsequent hydrothermal processes. Compared with FeOOH/$BiVO_4$/WO_3, $BiVO_4$/WO_3 and pure photoanodes, the photocurrent of F:FeOOH/$BiVO_4$/WO_3 photoelectrode is greatly improved, reaching 3.1 mA/cm^2 at 1.23 V vs. RHE, which is 7 times and 9 times than that of WO_3 and $BiVO_4$, respectively , and the initial potential also has a significant negative shift, showing remarkable PEC performance. This is mainly due to the appropriate energy band location between F:FeOOH/$BiVO_4$/WO_3 layers, which by a long way promotes the separation of electron-hole pairs, improves the efficiency of light utilization and surface charge injection, and facilitates the reaction kinetics on the surface of materials. In addition, according to the theoretical calculation results, F-doped FeOOH should have better OER catalytic performance than FeOOH, which is consistent with the experimental results. This method of combining suitable semiconductors into a multiheterostructure photoanode shows excellent performance in PEC water splitting, and has potential cost-effective and efficient PEC applications. It provides some ideas for further exploration of the construction of heterojunction of new photoanodes.

CRediT authorship contribution statement

Yan Li and **Qizhao Wang**: Methodology, Research, Writing – original draft, Funding acquisition, review & revised. **Qiong Mei, Zejun Liu** and **Zhaohui Zhou**: Theoretical calculation, Revised. **Xingsheng Hu** and **Jingwei Huang**: Discussion and drawing of mechanism diagram. **Bo Bai** and **Hui Liu**: Validation and Data management.

Declaration of Competing Interest

The authors declare that they have no known competing financial interests or personal relationships that could have appeared to influence the work reported in this paper.

Acknowledgements

This work was financially supported by the National Natural Science Foundation of China (No. 52173277, 21663027 and 21808189), the Fundamental Research Funds for the Central Universities of Chang'an University (No. 300102299304, 300102291403) and the Natural Science Basic Research Fund of Shaanxi Province (No. 2020JZ20).

Appendix A. Supporting information

Supplementary data associated with this article can be found in the online version at doi:10.1016/j.apcatb.2021.120995.

References

[1] Y. Chen, M. Xu, J. Wen, Y. Wan, Q. Zhao, X. Cao, Y. Ding, Z. Wang, H. Li, Z. Bian, Selective recovery of precious metals through photocatalysis, Nat. Sustain. 4 (2021) 618–626, https://doi.org/10.1038/s41893-021-00697-4.

[2] Q. Li, Y. Wang, J. Zeng, Q. Wu, Q. Wang, L. Sun, L. Xu, T. Ye, X. Zhao, L. Chen, Z. Chen, L. Chen, Y. Lei, Phosphating-induced charge transfer on CoO/CoP interface for alkaline H_2 evolution, Chin. Chem. Lett. (2021), https://doi.org/10.1016/j.cclet.2021.03.063.

[3] X. Deng, Y. Chen, J. Wen, Y. Xu, J. Zhu, Z. Bian, Polyaniline-TiO_2 composite photocatalysts for light-driven hexavalent chromium ions reduction, Sci. Bull. 65 (2020) 105–112, https://doi.org/10.1016/j.scib.2019.10.020.

[4] X. Hu, Q. Wang, Y. Li, Y. Meng, L. Wang, H. She, J. Huang, The hydrophilic treatment of a novel co-catalyst for greatly improving the solar water splitting performance over Mo-doped bismuth vanadate, J. Colloid Interface Sci. 607 (2021) 219–228, https://doi.org/10.1016/j.jcis.2021.08.195.

[5] J. Wen, L. Ling, Y. Chen, Z. Bian, Pyroelectricity effect on photoactivating palladium nanoparticles in $PbTiO_3$ for Suzuki coupling reaction, Chin. J. Catal. 41 (2020) 1674–1681, https://doi.org/10.1016/S1872-2067(20)63581-1.

[6] H. Chang, Z. Shang, Q. Kong, P. Liu, J. Liu, H. Luo, α-Fe_2O_3 nanorods embedded with two-dimensional {0 0 1} facets exposed TiO_2 flakes derived from Ti_3C_2TX MXene for enhanced photoelectrochemical water oxidation, Chem. Eng. J. 370 (2019) 314–321, https://doi.org/10.1016/j.cej.2019.03.181.

[7] J. Li, J. Li, H. Yuan, W. Zhang, Z. Jiao, X. Zhao, Modification of $BiVO_4$ with partially covered α-Fe_2O_3 spindles serving as hole-transport channels for significantly improved photoelectrochemical performance, Chem. Eng. J. 398 (2020), 125662, https://doi.org/10.1016/j.cej.2020.125662.

[8] Y. Chen, K. Yang, C. Huang, Z. Wu, Y. Hsu, Overall photoelectrochemical water splitting at low applied potential over ZnO quantum dots/nanorods homojunction, Chem. Eng. J. 368 (2019) 746–753, https://doi.org/10.1016/j.cej.2019.03.024.

[9] Y. Li, Q. Wang, X. Hu, Y. Meng, H. She, J. Huang, L. Wang, G. Zhu, Constructing NiFe-metal-organic frameworks from NiFe-layered double hydroxide as a highly efficient cocatalyst for $BiVO_4$ photoanode PEC water splitting, Chem. Eng. J. (2021), 133592 https://doi.org/0.1016/j.cej.2021.133592.

[10] S. Zhou, K. Chen, J. Huang, L. Wang, M. Zhang, B. Bai, H. Liu, Q. Wang, Preparation of heterometallic CoNi-MOFs-modified $BiVO_4$: a steady photoanode for improved performance in photoelectrochemical water splitting, Appl. Catal. B: Environ. 266 (2020), 118513, https://doi.org/10.1016/j.apcatb.2019.118513.

[11] D. Coelho, R.S. Gaudêncio, S.A. Carminati, W.P. Ribeiro, A.F. Nogueira, L. H. Mascaro, Bi electrodeposition on WO_3 photoanode to improve the photoactivity of the WO_3/$BiVO_4$ heterostructure to water splitting, Chem. Eng. J. 399 (2020), 125836, https://doi.org/10.1016/j.cej.2020.125836.

[12] J. Huang, Y. Wang, K. Chen, T. Liu, Q. Wang, H. Cheng, Boosting the photoelectrochemical water oxidation performance of bismuth vanadate by $ZnCo_2O_4$ nanoparticle, Chin. Chem. Lett. (2021), https://doi.org/10.1016/j.cclet.2021.08.082.

[13] G. Zhao, W. Ma, X. Wang, Y. Xing, S. Hao, X. Xu, Self-water-absorption-type two-dimensional composite photocatalyst with high-efficiency water absorption and overall water-splitting performance, Adv. Powder Metall. (2021) https://doi.org/110.1016/j.apmate.2021.09.008.

[14] H. She, M. Jiang, P. Yue, J. Huang, L. Wang, J. Li, G. Zhu, Q. Wang, Metal (Ni^{2+}/Co^{2+}) sulfides modified $BiVO_4$ for effective improvement in photoelectrochemical water splitting, J. Colloid Interface Sci. 549 (2019) 80–88, https://doi.org/10.1016/j.jcis.2019.04.038.

[15] J. Huang, T. Liu, R. Wang, M. Zhang, L. Wang, H. She, Q. Wang, Facile loading of cobalt oxide on bismuth vanadate: proved construction of p-n junction for efficient photoelectrochemical water oxidation, J. Colloid Interface Sci. 570 (2020) 89–98, https://doi.org/10.1016/j.jcis.2020.02.109.

[16] J. Zhang, G. Zhu, W. Liu, Y. Xi, D.A. Golosov, S.M Zavadski, S.N. Melnikov, 3D core-shell WO_3@α-Fe_2O_3 photoanode modified by ultrathin FeOOH layer for enhanced photoelectrochemical performances, J. Alloy. Compd. 834 (2020), 154992, https://doi.org/10.1016/j.jallcom.2020.154992.

[17] J. Feng, H. Huang, W. Guo, X. Xu, Y. Yao, Z. Yu, Z. Li, Z. Zou, Evaluating the promotional effects of WO_3 underlayers in $BiVO_4$ water splitting photoanodes, Chem. Eng. J. 417 (2021), 128095, https://doi.org/10.1016/j.cej.2020.128095.

[18] H. Sun, W. Hua, Y. Li, J. Wang, Promoting photoelectrochemical activity and stability of WO_3/$BiVO_4$ heterojunctions by coating a tannin nickel iron complex, ACS Sustain. Chem. Eng. 33 (2020) 12637–12645, https://doi.org/10.1021/acssuschemeng.0c04204.

[19] Y. Lan, Z. Liu, Z. Guo, X. Li, L. Zhao, L. Zhan, M. Zhang, A ZnO/$ZnFe_2O_4$ uniform core-shell heterojunction with a tubular structure modified by NiOOH for efficient photoelectrochemical water splitting, Dalton Trans. 47 (2018) 12181–12187, https://doi.org/10.1039/c8dt02581a.

[20] X. Feng, Y. Chen, Z. Qin, M. Wang, L. Guo, Facile fabrication of sandwich structured WO_3 nanoplate arrays for efficient photoelectrochemical water splitting, ACS Appl. Mater. Interfaces 28 (2016) 18089–18096, https://doi.org/10.1021/acsami.6b04887.

[21] J. Huang, Y. Zhang, Y. Ding, Rationally designed/constructed CoO_x/WO_3 anode for efficient photoelectrochemical water oxidation, ACS Catal. 7 (2017) 1841–1845, https://doi.org/10.1021/acscatal.7b00022.

[22] A.A. Markhabayeva, M. Moniruddin, R. Dupre, K.A. Abdullin, N. Nuraje, Designing of WO_3@Co_3O_4 heterostructures to enhance photoelectrochemical performances, J. Phys. Chem. A 124 (2020) 486–491, https://doi.org/10.1021/acs.jpca.9b09173.

[23] F.F. Abdi, L. Han, A.H. Smets, M. Zeman, B. Dam, R. Krol, Efficient solar water splitting by enhanced charge separation in a bismuth vanadate-silicon tandem photoelectrode, Nat. Commun. 4 (2013) 2195, https://doi.org/10.1038/ncomms3195.

[24] L. Wang, X. Shi, Y. Jia, H. Cheng, L. Wang, Q. Wang, Recent advances in bismuth vanadate-based photocatalysts for photoelectrochemical water splitting, Chin. Chem. Lett. 32 (2021) 1869–1878, https://doi.org/10.1016/j.cclet.2020.11.065.

[25] Y.O. Kim, S. Yu, K.S. Ahn, S.K. Lee, S. Kang, Enhancing the photoresponse of electrodeposited WO_3 film: structure and thickness effect, J. Electroanal. Chem. 752 (2015) 25–32, https://doi.org/10.1016/j.jelechem.2015.05.031.

[26] H.S. Park, K.E. Kweon, H. Ye, E. Paek, G.S. Hwang, A.J. Bard, Factors in the metal doping of $BiVO_4$ for improved photoelectrocatalytic activity as studied by scanning electrochemical microscopy and first-principles density-functional calculation, J. Phys. Chem. C. 115 (2011) 17870–17879, https://doi.org/10.1021/jp204492r.

[27] C. Liu, Y. Yang, J. Li, S. Chen, W. Li, X. Tang, An in situ transformation approach for fabrication of $BiVO_4$/WO_3 heterojunction photoanode with high photoelectrochemical activity, Chem. Eng. J. 326 (2017) 603–611, https://doi.org/10.1016/j.cej.2017.05.179.

[28] T.N. Thuy, S.K. Cho, Y. Amangeldinova, D. Yoo, G. Tukyei, Y. Sissembayeva, T. S. Atabaev, D. Lee, J. Lee, N.D. Nguyen, H.K. Kim, D.M. Shin, Y.H. Hwang, WO_3-ZnO and CuO-ZnO nanocomposites as highly efficient photoanodes under visible light illumination, Nanotechnology 31 (2020), 255702, https://doi.org/10.1088/1361-6528/ab7d75.

[29] K.H. Ng, L.J. Minggu, W.F. Lee, K. Arifin, M.H. Jumali, M.B. Kassim, A new method for the fabrication of a bilayer WO_3/Fe_2O_3 photoelectrode for enhanced photoelectrochemical performance, Mater. Res. Bull. 98 (2018) 47–52, https://doi.org/10.1016/j.materresbull.2017.04.019.

[30] Y. Wang, W. Tian, L. Chen, F. Cao, J. Guo, L. Li, Three-dimensional WO_3 nanoplate/Bi_2S_3 nanorod heterojunction as a highly efficient photoanode for improved photoelectrochemical water splitting, ACS Appl. Mater. Interfaces 46 (2017) 40235–40243, https://doi.org/10.1021/acsami.7b11510.

[31] Y. Lu, Y. Li, Y. Wang, J. Zhang, Two-photon induced NIR active core-shell structured WO_3/CdS for enhanced solar light photocatalytic performance, Appl. Catal. B: Environ. 272 (2020), 118979, https://doi.org/10.1016/j.apcatb.2020.118979.

[32] I. Fujimoto, N. Wang, R. Saito, Y. Miseki, T. Gunji, K. Sayama, WO_3/$BiVO_4$ composite photoelectrode prepared by improved auto-combustion method for highly efficient water splitting, Int. J. Hydrog. Energ. 39 (2014) 2454–2461, https://doi.org/10.1016/j.ijhydene.2013.08.114.

[33] X. Zhang, X. Wang, D. Wang, J. Ye, Conformal $BiVO_4$-layer/WO_3-nanoplate-array heterojunction photoanode modified with cobalt phosphate cocatalyst for significantly enhanced photoelectrochemical performances, ACS Appl. Mater. Interfaces 11 (2019) 5623–5631, https://doi.org/10.1021/acsami.8b05477.

[34] I. Grigioni, K.G. Stamplecoskie, E. Selli, P.V. Kamat, Dynamics of photogenerated charge carriers in wo3/bivo4 heterojunction photoanodes, J. Phys. Chem. C. 119 (2015) 20792–20800, https://doi.org/10.1021/acs.jpcc.5b05128.

[35] S. Bhat, S. Lee, J. Suh, S. Hong, H. Jang, Triple planar heterojunction of SnO_2/WO_3/$BiVO_4$ with enhanced photoelectrochemical performance under front illumination, Appl. Sci. 8 (2018) 1765, https://doi.org/10.3390/app8101765.

[36] Y. Liu, B.R. Wygant, K. Kawashima, O. Mabayoje, T.E. Hong, S.G. Lee, J. Lin, J. H. Kim, K. Yubuta, W. Li, J. Li, C.B. Mullins, Facet effect on the photoelectrochemical performance of a WO_3/$BiVO_4$ heterojunction photoanode, Appl. Catal. B: Environ. 245 (2019) 227–239, https://doi.org/10.1016/j.apcatb.2018.12.058.

[37] P. Wu, Z. Liu, D. Chen, M. Zhou, J. Wei, Flake-like NiO/WO_3 p-n heterojunction photocathode for photoelectrochemical water splitting, Appl. Surf. Sci. 440 (2018) 1101–1106, https://doi.org/10.1016/j.apsusc.2018.01.292.

[38] S. Khoomortezaei, H. Abdizadeh, M.R. Golobostanfard, Triple layer heterojunction WO_3/$BiVO_4$/$BiFeO_3$ porous photoanode for efficient photoelectrochemical water splitting, ACS Appl. Energy Mater. 9 (2019) 6428–6439, https://doi.org/10.1021/acsaem.9b01041.

[39] L. Zhou, Y. Wu, L. Wang, Y. Yang, Y. Na, Excellent performance of water oxidation at low bias potential achieved by transparent WO_3/$BiVO_4$ photoanode integrated with molecular nickel porphyrin, Inorg. Chem. Commun. 107 (2019), 107480, https://doi.org/10.1016/j.inoche.2019.107480.

[40] Z. Ma, H. Hou, K. Song, Z. Fang, L. Wang, F. Gao, Z. Yang, B. Tang, W. Yang, Ternary WO_3/porous-$BiVO_4$/FeOOH hierarchical architectures: towards highly efficient photoelectrochemical performance, ChemElectroChem 5 (2018) 3660–3667, https://doi.org/10.1002/celc.201801233.

[41] T. Zhou, S. Chen, J. Wang, Y. Zhang, J. Li, J. Bai, B. Zhou, Dramatically enhanced solar-driven water splitting of $BiVO_4$ photoanode via strengthening hole transfer and light harvesting by co-modification of CQDs and ultrathin β-FeOOH layers, Chem. Eng. J. 403 (2021), 126350, https://doi.org/10.1016/j.cej.2020.126350.

[42] J. Zhang, Z. Liu, Z. Liu, Novel WO_3/Sb_2S_3 heterojunction photocatalyst based on WO_3 of different morphologies for enhanced efficiency in photoelectrochemical water splitting, ACS Appl. Mater. Interfaces 15 (2016) 9684–9691, https://doi.org/10.1021/acsami.6b00429.

[43] C. Ta, C. Akamoto, Y. Furusho, F. Amano, A macroporous-structured WO_3/Mo-doped $BiVO_4$ photoanode for vapor-fed water splitting under visible light irradiation, ACS Sustain. Chem. Eng. 25 (2020) 9456–9463, https://doi.org/10.1021/acssuschemeng.0c02331.

[44] J. Deng, Q. Zhang, K. Feng, H. Lan, J. Zhong, M. Chaker, D. Ma, Efficient photoelectrochemical water oxidation on hematite with fluorine-doped FeOOH and FeNiOOH as dual cocatalysts, ChemSusChem 21 (2018) 3783–3789, https://doi.org/10.1002/cssc.201801751.

[45] Y. Li, X. Hu, J. Huang, L. Wang, H. She, Q. Wang, Development of iron-based heterogeneous cocatalysts for photoelectrochemical water oxidation, Acta Phys. Chim. Sin. 37 (2020), 2009022, https://doi.org/10.3866/PKU.WHXB202009022.

[46] W. Zhang, J. Ma, L. Xiong, H. Jiang, J. Tang, Well-crystallized α-FeOOH cocatalysts modified $BiVO_4$ photoanodes for efficient and stable photoelectrochemical water splitting, ACS Appl. Energy Mater. 6 (2020) 5927–5936, https://doi.org/10.1021/acsaem.0c00834.

[47] W. Chemelewski, J. Rosenstock, C. Mullins, Electrodeposition of Ni-doped FeOOH oxygen evolution reaction catalyst for photoelectrochemical water splitting, J. Mater. Chem. A 2 (2014) 14957–14962, https://doi.org/10.1039/c4ta03078h.

[48] L. Cai, J. Zhao, H. Li, J. Park, I. Cho, H. Han, X. Zheng, One-step hydrothermal deposition of Ni:FeOOH onto photoanodes for enhanced water oxidation, ACS Energy Lett. 1 (2016) 624–632, https://doi.org/10.1021/acsenergylett.6b00303.

[49] G. Chen, Y. Luo, L. Ding, H. Wang, Low-voltage electrolytic hydrogen production derived from efficient water and ethanol oxidation on fluorine-modified FeOOH anode, ACS Catal. 8 (2017) 526–530, https://doi.org/10.1021/acscatal.7b03319.

[50] Q. Zeng, J. Li, L. Li, J. Bai, L. Xia, B. Zhou, Synthesis of $WO_3/BiVO_4$ photoanode using a reaction of bismuth nitrate with peroxovanadate on WO_3 film for efficient photoelectrocatalytic water splitting and organic pollutant degradation, Appl. Catal. B Environ. 217 (2017) 21–29, https://doi.org/10.1016/j.apcatb.2017.05.072.

[51] R. Guo, Y. He, T. Yu, P. Cheng, J. You, C. Chen, T. Chan, X. Liu, Z. Hu, Enhanced oxygen evolution reaction activity of flower-like FeOOH via the synergistic effect of sulfur, Chem. Eng. J. 420 (2021), 127587, https://doi.org/10.1016/j.cej.2020.127587.